Research Square

Preprints are preliminary reports that have not undergone peer review.
They should not be considered conclusive, used to inform clinical practice,
or referenced by the media as validated information.

Pseudohalide dependent assembly of discrete zinc(II) clusters and one-dimensional coordination polymers with a cyclohexanediamine-derived Schiff base: Crystal structures, characterization and antibacterial activity

Chun-Hua Dai

yctudai@163.com

Yancheng Teachers University

Fu-Lin Mao

Yancheng Teachers University

Research Article

Keywords: Zinc(II) complex, Schiff base, Pseudohalide, Reactant stoichiometry, Antibacterial activity

Posted Date: November 10th, 2026

DOI: https://doi.org/10.21203/rs.3.rs-11460948/v1

License: This work is licensed under a Creative Commons Attribution 4.0 International License.
Read Full License

Additional Declarations: No competing interests reported.

Pseudohalide dependent assembly of discrete zinc(II) clusters and one-dimensional coordination polymers with a cyclohexanediamine-derived Schiff base: Crystal structures, characterization and antibacterial activity

Chun-Hua Dai*, Fu-Lin Mao

School of Chemical and Environmental Engineering, Yancheng Teachers University, Yancheng 224002, PR China

** Corresponding author email: yctudai@163.com*

Abstract

A tetradentate Schiff base, H_2L, obtained from 5-methoxysalicylaldehyde and cyclohexane-1,2-diamine, afforded five zinc(II) complexes with distinct nuclearities and connectivities. Reaction with zinc acetate in methanol gave the discrete trinuclear complex $[Zn_3L_2(OAc)_2]$ (**1**). At H_2L:Zn:azide ratios of 1:2:1 and 1:2:2, respectively, tetranuclear $[Zn_4L_2(OAc)_2(N_3)_2]$ (**2**) and $[Zn_4L_2(N_3)_4]$ (**3**) were obtained. Corresponding dicyanamide reactions yielded one-dimensional $[Zn_3L_2(dca)_2]_n$ (**4**) and $[Zn_2L(dca)_2]_n$ (**5**), where dca = $N(CN)_2$. Thus, increased pseudohalide loading is associated with acetate exclusion in the azide series and a change from trinuclear to dinuclear repeat units in the dicyanamide series. The compounds were characterized by spectroscopic methods as well as single crystal X-ray diffraction. Antibacterial activities of the compounds were studied. At 1.0 mg mL^{-1}, complex **2** produced the largest mean inhibition zones among the complexes against *S. aureus* and *B. subtilis*, measuring 26 ± 4 and 28 ± 5 mm, respectively.

Keywords: Zinc(II) complex; Schiff base; Pseudohalide; Reactant stoichiometry; Antibacterial activity

Introduction

Schiff bases provide a versatile connection between organic molecular design and metal-directed assembly. A great number of Schiff base complexes have been reported for their versatile structures and interesting applications [1-3]. Salicylaldehyde-derived ligands are especially useful because deprotonation places a phenoxide donor adjacent to the imine nitrogen. When two such units are joined through a diamine, the resulting N_2O_2 donor set can bind one metal ion while the phenoxide oxygen atoms remain available to bridge additional metal centers [4,5]. A tetradentate ligand can therefore support structures whose nuclearity exceeds that suggested by a simple one-metal chelate. This distinction between the primary

chelation site and secondary bridging sites is central to the assembly chemistry of salen-type ligands.

Zinc(II) with d^{10} configuration accommodates several coordination numbers and does not impose the ligand-field preferences characteristic of many open-shell transition metal ions. Four-, five- and six-coordinate environments can therefore coexist within related zinc assemblies [6,7]. Acetate adds a further variable because it can supply charge compensation and connect metal centres through its oxygen donors [8]. A zinc acetate precursor consequently serves both as a source of Zn^{2+} and as a potential source of a structural ligand. Pseudohalides provide a complementary route to controlling connectivity. Azide can bind terminally or bridge through one or both ends, and modest changes in its availability can alter the donor environment around an existing metal–phenoxide framework [9]. Dicyanamide offers two terminal nitrile nitrogen atoms separated by a central nitrogen, allowing connections that extend beyond a compact metal cluster [10]. Zinc Schiff base chemistry already includes polynuclear azido species and dicyanamide-linked assemblies, including extended structures [11,12]. The relevant question is therefore not whether either anion can bridge zinc, but how its identity and loading change the balance between a finite cluster and an extended coordination architecture within the same ligand–metal platform.

Schiff bases and their metal complexes have also attracted attention as antibacterial agents [13,14]. Their activity can depend on ligand substitution, metal availability, solubility and the species generated in the assay medium. Zinc compounds are of particular interest because perturbation of zinc homeostasis can affect bacterial physiology even though Zn^{2+} is not a redox-cycling ion under ordinary biological conditions. A number of Schiff base zinc complexes have been reported to possess excellent antibacterial activities [15-17].

In this work, H_2L is combined with zinc acetate at a constant ligand:metal feed ratio of 1:2, and the added sodium pseudohalide is varied between zero, one and two equivalents per ligand. This design separates the acetate-containing baseline from azide and dicyanamide branches. The principal objective is to determine how these feed compositions are associated with acetate retention, zinc coordination geometry, metal-core nuclearity and propagation into chains or networks.

Experimental

Materials and measurements

5-Methoxysalicylaldehyde and cyclohexane-1,2-diamine were available from Alfa Aesar Company and used without purification. Zinc acetate, sodium azide and sodium dicyanamide were purchased from Beijing Chemical Reagent Company and used as received. Gatifloxacin

and Ciprofloxacin were purchased in powder form from Aladin Chemical Reagent Co. Ltd. Carbon, hydrogen and nitrogen were determined on a Perkin-Elmer 240C microanalyser. IR spectra (4000–400 cm^{-1}) as KBr pellets were recorded on a Nicolet FT-IR 170X spectrophotometer. UV-Vis spectra were obtained on a Lambda 35 spectrometer. Powder XRD data were collected on a Bruker D8 Advance X-ray diffractometer using Cu Kα radiation (λ = 1.548 Å) generated at 40 kV and 40 mA. The powder XRD spectra were recorded using a 1D Lynxeye detector under ambient conditions. ^{1}H and ^{13}C NMR spectra were performed with a Bruker 500 MHz instrument. X-ray diffraction was carried out on a Bruker APEX II CCD diffractometer.

Synthesis of H_2L

To a methanolic solution (30 mL) of 5-methoxysalicylaldehyde (0.020 mol, 3.0 g) was added a methanolic solution of cyclohexane-1,2-diamine (0.010 mol, 1.1 g) with stirring. The mixture was stirred for 30 min at reflux and with the solvent removed by distillation under reduced pressure. The solid was re-crystallized from methanol to give colorless crystalline product. Yield: 3.2 g (84%). Anal. calc. for $C_{22}H_{26}N_2O_4$: C, 69.09; H, 6.85; N, 7.32%. Found: C, 68.83; H, 6.91; N, 7.27%. ^{1}H NMR (500 MHz, DMSO-d_6): δ 12.67 (s, 2H, OH), 8.44 (s, 2H, CH=N), 6.93 (d, J = 3.2 Hz, 2H, ArH), 6.89 (dd, J = 8.8, 3.2 Hz, 2H, ArH), 6.75 (d, J = 8.8 Hz, 2H, ArH), 3.66 (s, 6H, OCH_3), 3.39–3.37 (m, 2H, NCH), 1.88–1.79 (m, 4H, cyclohexyl CH_2), 1.63–1.44 (m, 4H, cyclohexyl CH_2). ^{13}C NMR (126 MHz, DMSO-d_6): δ 164.65, 154.18, 151.48, 119.09, 118.27, 116.98, 114.89, 71.54, 55.45, 32.50, 23.66. Selected IR bands (KBr, cm^{-1}): 2932, 2858, 1636, 1591, 1495, 1269, 1221, 1161, 1036, 822. UV–Vis data (λ_{max}, nm): 229, 257, 345.

Synthesis of the complexes

$[Zn_3L_2(OAc)_2]$ (1)

H_2L (1.0 mmol, 0.38 g) was dissolved in methanol (50 mL), to which was added zinc acetate dihydrate (2.0 mmol, 0.44 g). The mixture was stirred at room temperature for 30 min to give a clear colorless solution. Single crystals of the complex were grown from the solution upon slow evaporation within a week. The crystals were isolated by filtration, washed with cold methanol and dried in vacuum containing anhydrous $CaCl_2$. Yield: 0.39 g (72%). Anal. calc. for $C_{48}H_{54}N_4O_{12}Zn_3$: C, 53.62; H, 5.06; N, 5.21%. Found: C, 53.45; H, 5.12; N, 5.28%. Selected IR bands (KBr, cm^{-1}): 1636, 1614, 1578, 1541, 1477, 1437, 1385, 1283, 1219, 1159, 1038, 839, 802. UV–Vis data (λ_{max}, nm): 226, 247, 378.

$[Zn_4L_2(OAc)_2(N_3)_2]$ (2)

H_2L (1.0 mmol, 0.38 g), zinc acetate dihydrate (2.0 mmol, 0.44 g) and sodium azide (1.0 mmol, 0.065 g) were reacted in methanol (50 mL) at room temperature for 30 min, followed by slow

evaporation to afford colorless single crystals. Yield: 0.41 g (67%). Anal. calc. for $C_{48}H_{54}N_{10}O_{12}Zn_4$: C, 47.08; H, 4.45; N, 11.44%. Found: C, 47.22; H, 4.38; N, 11.32%. Selected IR bands (KBr, cm^{-1}): 2098, 1639, 1612, 1555, 1479, 1423, 1389, 1275, 1223, 1161, 1034, 802. UV–Vis data (λ_{max}, nm): 226, 246, 380.

$[Zn_4L_2(N_3)_4]$ (3)

H_2L (1.0 mmol, 0.38 g), zinc acetate dihydrate (2.0 mmol, 0.44 g) and sodium azide (2.0 mmol, 0.13 g) were reacted in methanol (50 mL) at room temperature for 30 min, followed by slow evaporation to afford colorless single crystals. Yield: 0.46 g (77%). Anal. calc. for $C_{44}H_{48}N_{16}O_8Zn_4$: C, 44.39; H, 4.06; N, 18.83%. Found: C, 44.30; H, 4.12; N, 18.71%. Selected IR bands (KBr, cm^{-1}): 2096, 2058, 1640, 1555, 1481, 1384, 1275, 1225, 1160, 1038, 801. UV–Vis data (λ_{max}, nm): 226, 246, 379.

$[Zn_3L_2(dca)_2]_n$ (4)

H_2L (1.0 mmol, 0.38 g), zinc acetate dihydrate (2.0 mmol, 0.44 g) and sodium dicyanamide (1.0 mmol, 0.089 g) were reacted in methanol (50 mL) at room temperature for 30 min, followed by slow evaporation to afford colorless single crystals. Yield: 0.33 g (61%). Anal. calc. for $C_{48}H_{48}N_{10}O_8Zn_3$: C, 52.93; H, 4.44; N, 12.86%. Found: C, 52.68; H, 4.40; N, 12.75%. Selected IR bands (KBr, cm^{-1}): 2326, 2262, 2210, 2196, 1641, 1615, 1563, 1547, 1478, 1382, 1278, 1220, 1161, 1038. UV–Vis data (λ_{max}, nm): 225, 246, 377.

$[Zn_2L(dca)_2]_n$ (5)

H_2L (1.0 mmol, 0.38 g), zinc acetate dihydrate (2.0 mmol, 0.44 g) and sodium dicyanamide (2.0 mmol, 0.18 g) were reacted in methanol (50 mL) at room temperature for 30 min, followed by slow evaporation to afford colorless single crystals. Yield: 0.46 g (72%). Anal. calc. for $C_{26}H_{24}N_8O_4Zn_2$: C, 48.55; H, 3.76; N, 17.42%. Found: C, 48.71; H, 3.85; N, 17.34%. Selected IR bands (KBr, cm^{-1}): 2325, 2262, 2212, 2197, 1641, 1615, 1546, 1478, 1381, 1278, 1220, 1161, 1038. UV–Vis data (λ_{max}, nm): 226, 246, 377.

X-ray crystallography

Single crystal X-ray diffraction data for complexes **1**–**5** were collected at 298(2) K using Mo Kα radiation (λ = 0.71073 Å) on a Bruker APEX II CCD diffractometer equipped with a graphite monochromator. The data were corrected for Lorentz and polarization effects and for absorption. The structures were solved using SHELXT [18] and refined against F^2 by full-matrix least-squares methods using SHELXL-2014/7 [19]. Non-hydrogen atoms were refined anisotropically, and hydrogen atoms were placed in calculated positions and refined using a riding model. In **1**, the C8–C13 cyclohexane ring was modelled over two alternative conformations with refined occupancies of 0.347(8) and 0.653(8). In **2**, the C8–C13 fragment and the C17–C20/O4/C22 fragment were modelled over alternative sites with occupancies of

0.810(6)/0.190(6) and 0.40(3)/0.60(3), respectively. Similarity restraints were applied to the displacement parameters of disordered atoms in **1** and **2**. In **4**, the disordered ligand was refined over two conformations with occupancies of 0.406(18) and 0.594(18); the displacement parameters of corresponding alternative N atoms were constrained to be equal. Crystal data and refinement parameters are listed in Table 1, and selected bond lengths and angles are given in Table 2.

Antibacterial screening

Antibiograms of H_2L, the five complexes and two reference antibiotics Gatifloxacin and Ciprofloxacin were assayed against two Gram-positive bacteria *Staphylococcus aureus* and *Bacillus subtilis* and two Gram-negative bacteria *Pseudomonas aeruginosa* and *Escherichia coli* using the agar well diffusion method on nutrient agar medium [20]. During the experiment, the test microbes were removed from the slant aseptically with inoculating loops and transferred to separate test tubes containing a solution of 0.85% NaCl (5.0 mL). Sufficient inoculums were then added to adjust the turbidity to 0.5 McFarland (108 CFU mL^{-1}). The suspension (1.0 mL) was added to 15–20 mL of nutrient agar and transferred to an agar plate of 9.0 cm diameter for each bacterium. The antibacterial activities of the compounds were tested after cooling the inoculated agar at room temperature for 25 min. The antibacterial activities of the tested materials were also evaluated during the same condition. The tested materials were dissolved in DMSO to prepare five different concentrations (0.2, 0.4, 0.6, 0.8 and 1.0 mg mL^{-1}) for evaluation of limiting doses. Wells of 0.6 cm diameter were pierced in the agar and filled with the test materials of varied concentrations and incubated for 24 h at 310(2) K for the bacterial strains. Antibacterial activities were evaluated by measuring the inhibition zone diameters (IZDs) and the lowest tested concentrations producing measurable inhibition zones. Each experiment was repeated thrice along with a control set using DMSO. The mean value obtained for three individual replicates was then used to calculate the growth inhibition zone of each sample.

Results and discussion

Chemistry

Condensation of 5-methoxysalicylaldehyde and cyclohexane-1,2-diamine produces a bis(salicylidene) framework containing two phenolic groups, two imine donors and two peripheral methoxy groups. Removal of the phenolic protons upon complex formation gives L^{2-}, which binds zinc through its N_2O_2 pocket and also supplies phenoxide bridges.

In the absence of an added pseudohalide, **1** contains three zinc centres per two ligands, even though two equivalents of zinc acetate were supplied per H_2L. A feed composition need

not be retained quantitatively in the crystallizing phase, and the excess zinc cannot be assigned to a particular mother-liquor species from these data. Addition of one equivalent of azide per ligand produces **2**, in which acetate remains incorporated. Doubling the azide feed gives **3**, which contains four azides and no acetate per Zn_4L_2 unit. Thus, the experimentally observed change is substitution of the auxiliary-ligand inventory within a tetranuclear composition, rather than an increase in cluster nuclearity.

The dicyanamide branch follows a different pattern. Both **4** and **5** propagate through coordination bonds into one-dimensional structures. At the lower dicyanamide feed, the repeat composition contains a trinuclear Zn_3L_2 unit; at the higher feed, it contains a dinuclear Zn_2L unit. The dca:L ratio in the crystal product increases from 1:1 in **4** to 2:1 in **5**, whereas the metal:ligand ratio changes from 3:2 to 2:1. These observations identify a change in the building unit selected for chain growth. They do not support a general rule that greater pseudohalide loading necessarily increases dimensionality, since **4** and **5** have the same dimensionality.

The series therefore reveals two distinct structural responses to altered feed composition: acetate exclusion with rearrangement of a finite azido cluster, and reorganization of phenoxide-linked units within dicyanamide chains. All five structural formulations are electrically neutral and contain no separately required counterions.

NMR characterization of H_2L

The ^{1}H NMR spectrum provides complementary evidence for condensation and the resulting ligand symmetry (Figure S1). The two-proton singlet at δ 8.44 is assigned to the imine CH groups, while the strongly downfield signal at δ 12.67 is assigned to the two phenolic protons. Such deshielding may be consistent with intramolecular O–H···N interactions in the salicylidene units. The aromatic region contains three sets of resonances with the expected two-proton contributions. A small *meta* coupling near 3.2 Hz and an *ortho* coupling near 8.8 Hz account for the observed doublet–doublet of doublets–doublet pattern of the substituted rings. The methoxy groups give a six-proton singlet at δ 3.66. Signals at δ 3.39–3.37 arise from the cyclohexane methine positions bonded to the imine nitrogens, and the remaining ring protons occupy the δ 1.88–1.44 region. Reintegration of separate regions of the processed spectrum, normalized to two imine protons, gives approximate relative areas of 1.87, 2.00, 5.94, 5.97, 1.87 and 8.11 for OH, CH=N, aromatic H, OCH_3, NCH and cyclohexyl CH_2, respectively. Residual DMSO and water signals are distinguishable near δ 2.50 and 3.30.

Eleven principal ligand resonances are observed in the ^{13}C NMR spectrum, consistent with equivalence of the two molecular halves on the NMR timescale (Figure S2). The resonance at δ 164.65 is assigned to the imine carbon. The two oxygen-substituted aromatic

carbons occur at δ 154.18 and 151.48, and the remaining aromatic resonances lie between δ 114.89 and 119.09. Signals at δ 71.54 and 55.45 are consistent with N-bound methine and methoxy carbons, respectively, while δ 32.50 and 23.66 account for the cyclohexane methylene environments.

Crystal structure description of the complexes

In all five structures, the Schiff base ligand (L^{2-}) coordinates through its two imine N atoms and two phenoxide O atoms, with the phenoxide donors additionally linking zinc centers. The five-coordinate geometries are described using $\tau_5 = (\beta - \alpha)/60$, where β and α are the largest and second-largest donor–metal–donor angles, respectively; the ideal square-pyramidal and trigonal-bipyramidal limits are 0 and 1 [21].

Complex 1

Complex **1** crystallizes in the monoclinic space group $P2_1/c$ (Z = 2) as a neutral, centrosymmetric trinuclear species, $[Zn_3L_2(OAc)_2]$ (Figure 1). The asymmetric unit contains one complete L^{2-} ligand, one acetate anion, a Zn1 atom on a general position and a Zn2 atom on an inversion center with a crystallographic contribution of one-half. The complete molecule is generated by the operation (i) $1 - x$, $1 - y$, $1 - z$. Each L^{2-} ligand chelates a terminal Zn1 center through its two imine N atoms and two phenoxide O atoms; both phenoxide donors also bind the central Zn2 center. Each acetate bridges the same terminal–central metal pair through O5 and O6. Thus, the molecule contains two equivalent terminal Zn1 sites surrounding a central Zn2 site, with a Zn1···Zn2 separation of 2.9806(3) Å and a Zn1–Zn2–$Zn1^{i}$ angle of 180°.

The terminal Zn1 center has an N_2O_3 donor environment with a distorted square-pyramidal arrangement. The ligand donors N1, N2, O1 and O2 form the basal donor set, and acetate O5 occupies the apical position. The Zn1–O1 and Zn1–O2 distances are 2.0254(19) and 2.002(2) Å, respectively, whereas Zn1–O5 is shorter at 1.977(2) Å. The imine Zn1–N1 and Zn1–N2 distances are 2.035(2) and 2.055(2) Å. The two largest donor–Zn1–donor angles are O2–Zn1–N1 = 149.29(10)° and O1–Zn1–N2 = 148.77(10)°, giving $\tau_5 = 0.009$. Although this value places the geometry near the square-pyramidal limit of the τ_5 scale, the individual angles show appreciable distortion: the O1–Zn1–O2 and N1–Zn1–N2 angles are 84.24(8) and 80.48(9)°, respectively.

The central Zn2 center is six-coordinate, with an O_6 environment supplied by four phenoxide O atoms from two L^{2-} ligands and two acetate O6 donors. The Zn2–O1 and Zn2–O2 distances are 2.1380(19) and 2.1207(17) Å, respectively, and both Zn2–O6 distances are 2.071(2) Å. Inversion symmetry places each donor opposite its equivalent, producing three *trans* angles of 180°; the remaining angles span 78.72(7)–101.28(7)°. The resulting

coordination polyhedron is a distorted octahedron. The two phenoxide bridge angles, Zn1–O1–Zn2 and Zn1–O2–Zn2, are 91.39(8) and 92.57(8)°, respectively.

The acetate C23–O5 and C23–O6 distances are 1.265(3) and 1.244(4) Å. The ligand retains imine C7–N1 and C14–N2 distances of 1.266(4) and 1.270(4) Å, while its methoxy O atoms remain outside the metal coordination spheres. The cyclohexane fragment C8–C13 is modelled over two alternative conformations with occupancies of 0.347(8) and 0.653(8). This disorder concerns the ligand backbone and does not alter the trinuclear metal connectivity.

Complex 2

Complex **2** crystallizes in the triclinic space group *P*−1 (Z = 1) as the discrete tetranuclear species $[Zn_4L_2(OAc)_2(N_3)_2]$ (Figure 2). Its asymmetric unit consists of two independent zinc atoms, one L^{2-} ligand, one acetate and one azide. Inversion through (i) 1 − *x*, 2 − *y*, 1 − *z* generates the second half of the molecule. Within each Zn1/Zn2 pair, O1 and O2 act as phenoxide bridges, and the acetate additionally connects the metals through O5 and O6. Two symmetry-related azides join the inner Zn2 centers through their terminal N3 atoms in a $\mu_{1,1}$ end-on mode, completing the centrosymmetric tetranuclear assembly.

Zn1 is five-coordinate with an N_2O_3 donor set comprising N1, N2, O1 and O2 from L^{2-} and O5 from acetate. Its coordination sphere is a distorted square pyramid with acetate O5 in the apical position. The Zn1–O1 and Zn1–O2 distances are 2.023(3) and 2.024(3) Å, respectively, and Zn1–O5 is 1.995(3) Å. The Zn1–N1 and Zn1–N2 distances are 2.038(3) and 2.024(3) Å. The largest angles, O1–Zn1–N2 = 150.68(16)° and O2–Zn1–N1 = 143.68(15)°, yield τ_5 = 0.117. The O1–Zn1–O2 and N1–Zn1–N2 angles are 81.48(10) and 81.88(14)°, respectively.

Zn2 is also five-coordinate, but its O_3N_2 environment comprises two phenoxide donors, one acetate donor and two azide N atoms. The Zn2–O2, Zn2–O1 and Zn2–O6 distances are 2.001(3), 2.101(2) and 2.009(3) Å, respectively. The two azide contacts, Zn2–N3 and Zn2–$N3^i$, are unequal at 2.050(3) and 2.109(3) Å. Its two largest angles, O1–Zn2–$N3^i$ = 168.64(11)° and O6–Zn2–N3 = 140.37(14)°, give τ_5 = 0.471, indicating an intermediate geometry between the ideal square-pyramidal and trigonal-bipyramidal limits. The N3–Zn2–$N3^i$ angle is 77.43(15)°, and the complementary Zn2–N3–$Zn2^i$ bridge angle is 102.57(15)°.

The phenoxide-linked Zn1···Zn2 separation is 2.9148(6) Å, with Zn1–O1–Zn2 and Zn1–O2–Zn2 angles of 89.92(10) and 92.81(11)°, respectively. The acetate C–O distances are 1.256(5) and 1.261(5) Å, while the bridging azide has N3–N4 and N4–N5 distances of 1.202(5) and 1.122(5) Å. The cyclohexane fragment is disordered over two conformations with occupancies of 0.810(6) and 0.190(6). A second disordered region, comprising C17–

C20/O4/C22, has occupancies of 0.40(3) and 0.60(3). Both disorder components preserve the same metal–ligand connectivity.

Complex 3

Complex **3** crystallizes in the triclinic space group *P*−1 (Z = 1) and forms a centrosymmetric, discrete tetranuclear complex of composition $[Zn_4L_2(N_3)_4]$ (Figure 3). The asymmetric unit contains two independent zinc atoms, one L^{2-} ligand and two azides. The complete assembly is generated by (i) $1 - x$, $1 - y$, $1 - z$. The ligand binds Zn1 through its N_2O_2 donor pocket and connects it to Zn2 through both phenoxide O atoms. The N3–N4–N5 azide bridges Zn2 and $Zn1^{i}$ through N3 in a $\mu_{1,1}$ end-on mode. Its inversion-related counterpart provides the reciprocal connection, closing a tetranuclear metal-connectivity cycle. The second azide, N6–N7–N8, is terminally coordinated to Zn2 through N6; consequently, the full molecule contains two bridging and two terminal azides.

Zn1 has a five-coordinate N_3O_2 environment consisting of ligand donors N1, N2, O1 and O2 and the azide donor $N3^{i}$. The Zn1–O1 and Zn1–O2 distances are 2.023(3) and 2.007(3) Å, respectively, and the Zn1–N1 and Zn1–N2 distances are 2.052(3) and 2.038(3) Å. The additional $Zn1–N3^{i}$ contact measures 2.040(4) Å. The two largest coordination angles are O1–Zn1–N2 = 143.42(15)° and O2–Zn1–N1 = 141.55(15)°, giving $\tau_5 = 0.031$. The geometry is therefore described as a strongly distorted square pyramid, with $N3^{i}$ occupying the apical site. The O1–Zn1–O2 and N1–Zn1–N2 angles are 77.63(11) and 81.86(12)°, respectively.

Zn2 is four-coordinate with an N_2O_2 donor set comprising O1, O2, bridging-azide N3 and terminal-azide N6. Its Zn2–O1 and Zn2–O2 distances are 1.956(3) and 1.982(3) Å, respectively; Zn2–N3 and Zn2–N6 measure 1.981(3) and 1.966(5) Å. The donor–Zn2–donor angles range from 79.81(11)° for O1–Zn2–O2 to 121.8(2)° for O1–Zn2–N6, defining a distorted tetrahedral environment. The narrow O1–Zn2–O2 angle is associated with the doubly phenoxide-bridged Zn1/Zn2 unit. The metal separation within this unit is 3.0806(7) Å, and the Zn1–O1–Zn2 and Zn1–O2–Zn2 angles are 101.46(12) and 101.10(12)°, respectively.

The end-on bridge has a $Zn2–N3–Zn1^{i}$ angle of 124.35(17)°. The bridging azide N3–N4 and N4–N5 distances are 1.232(5) and 1.148(6) Å, whereas the terminal azide N6–N7 and N7–N8 distances are 1.178(8) and 1.190(8) Å. The imine distances C7–N1 and C14–N2 are 1.282(5) and 1.274(5) Å.

Complex 4

Complex **4** crystallizes in the monoclinic space group *P*2/*c* (Z = 2) as a one-dimensional coordination polymer, $[Zn_3L_2(dca)_2]_n$, where dca^{-} denotes dicyanamide (Figure 4). The asymmetric unit contains one L^{2-} ligand, one dca^{-} anion, one Zn1 atom on a general position and a Zn2 atom on a crystallographic twofold axis, corresponding to one-half of a trinuclear

repeat unit. Each ligand chelates Zn1 through its N_2O_2 donor set and bridges to a neighbouring Zn2 through O1 and O2. Two symmetry-related ligand-bound Zn1 centers surround Zn2 to form a bent trinuclear unit. The Zn1···Zn2 separation is 3.1480(9) Å, and the angle between the two Zn2-to-Zn1 vectors is 109.05(4)°. Dicyanamide bridges link these units into chains extending along [001].

Zn1 is five-coordinate with an N_3O_2 donor set. The ligand contributes O1, O2 and two imine N donors, and the terminal nitrile N3 atom of dca^- completes the coordination sphere. The Zn1–O1 and Zn1–O2 distances are 1.996(5) and 1.990(4) Å, respectively, while the two imine Zn–N distances are 2.049(5) and 2.051(6) Å for the corresponding alternative ligand sites. The Zn1–N3 distance is 1.990(6) Å. The largest coordination angles are O1–Zn1–N2 = 151.3(2)° and O2–Zn1–N1 = 142.9(2)°, giving $\tau_5 = 0.140$. This site is described as a distorted square pyramid with dca N3 in the apical position. The O1–Zn1–O2 and N1–Zn1–N2 angles are 84.09(18) and 79.8(2)°, respectively.

The central Zn2 site is six-coordinate, with an O_4N_2 donor environment formed by four phenoxide O atoms from two ligands and two symmetry-related terminal N5 donors from dca^-. The two pairs of phenoxide Zn–O distances are 2.134(4) and 2.151(5) Å, and both Zn2–N5 distances are 2.077(6) Å. The N5–Zn2–N5 angle of 89.9(3)° establishes a *cis* arrangement of the dicyanamide donors. The nearly *trans* N5–Zn2–O1 angles of 175.5(2)° and the O2–Zn2–O2 angle of 166.5(2)° indicate a distorted octahedral geometry. The phenoxide Zn1–O–Zn2 bridge angles are 99.3(2) and 98.9(2)°. For the Zn1 atom in the asymmetric unit, the phenoxide-linked Zn2 is generated by $1 - x$, $2 - y$, $1 - z$.

Each dca^- uses its two terminal nitrile N atoms, N3 and N5, to link Zn1 and Zn2 centers belonging to different trinuclear units; the central N4 atom is uncoordinated. The terminal C23–N3 and C24–N5 distances are 1.086(9) and 1.121(8) Å, respectively, and the C23–N4 and C24–N4 distances are 1.319(10) and 1.336(10) Å. The ligand backbone is modelled over two alternative conformations with occupancies of 0.406(18) and 0.594(18), including the alternative N1/N2 labels. These alternative sites represent mutually exclusive conformations and do not increase the coordination number of Zn1.

Complex 5

Complex **5** crystallizes in the triclinic space group $P\bar{1}$ (Z = 2) and forms a one-dimensional coordination polymer with repeat composition $[Zn_2L(dca)_2]_n$ (Figure 5). The asymmetric unit contains two crystallographically independent zinc atoms, one L^{2-} ligand and two dca^- anions. The ligand chelates Zn1 through N1, N2, O1 and O2, while O1 and O2 also bind $Zn2^i$ [symmetry code (i): $1 - x$, $1 - y$, $1 - z$]. Thus, the local phenoxide-bridged dinuclear unit

comprises Zn1 and a symmetry-related Zn2 atom. Its Zn1···Zn2^{i} separation is 3.1276(13) Å, with Zn1–O1–Zn2^{i} and Zn1–O2–Zn2^{i} angles of 101.3(2) and 102.3(2)°, respectively.

Zn1 has a five-coordinate N_3O_2 environment, with the four ligand donors forming the basal donor set and dca N3 occupying the apical position of a distorted square pyramid. The Zn1–O1 and Zn1–O2 distances are 2.000(5) and 1.997(5) Å, respectively. The imine Zn1–N1 and Zn1–N2 distances are 2.044(6) and 2.083(6) Å, and Zn1–N3 is 1.986(7) Å. The two largest angles, O2–Zn1–N1 = 146.0(3)° and O1–Zn1–N2 = 138.9(2)°, give τ_5 = 0.118. The phenoxide and imine donor-pair angles are O1–Zn1–O2 = 78.8(2)° and N1–Zn1–N2 = 80.1(3)°, respectively.

Zn2 is also five-coordinate with an N_3O_2 donor set, but its coordination sphere comprises two phenoxide donors from a symmetry-related ligand and three terminal nitrile N donors from dicyanamide ligands. The Zn2–O2^{i} and Zn2–O1^{i} distances are 2.020(5) and 2.044(5) Å, respectively. The dicyanamide contacts Zn2–N5, Zn2–N6 and Zn2–N8^{ii} measure 1.996(7), 2.043(8) and 2.105(8) Å [symmetry code (ii): 1 − *x*, 2 − *y*, − *z*]. The largest angles, O1^{i}–Zn2–N8^{ii} = 155.3(3)° and O2^{i}–Zn2–N6 = 140.2(3)°, yield τ_5 = 0.252. This geometry lies closer to the square-pyramidal limit, with N5 as the apical donor, but is substantially distorted; the O2^{i}–Zn2–O1^{i} angle is 77.3(2)°. Both metal sites therefore have the same coordination number and donor-atom composition but different donor origins and angular distortions.

The two independent dca^{-} ligands provide distinct connections. The N3–C23–N4–C24–N5 ligand connects Zn1 and Zn2 through its terminal N3 and N5 atoms, linking different phenoxide-bridged units. The N6–C25–N7–C26–N8 ligand bridges Zn2 and Zn2^{ii} through N6 and N8. Neither central N4 nor central N7 coordinates to zinc. Repetition of these connections generates the chain along [0 1 −1]. The terminal nitrile C–N distances span 1.109(10)–1.134(10) Å, and the C–N distances involving the central dca N atoms span 1.261(12)–1.284(11) Å. The ligand imine distances are 1.274(10) and 1.279(9) Å.

IR spectroscopy

The IR spectra show a common ligand fingerprint accompanied by anion-specific changes (Figures S3-S8). H_2L exhibits a prominent band at 1636 cm^{-1} assigned principally to the azomethine stretching vibration. Corresponding features occur at 1636, 1639, 1640, 1641 and 1641 cm^{-1} for **1**–**5**. The shifts are therefore small and predominantly towards higher wavenumber, not the uniform lowering sometimes associated with imine coordination. Since these modes can mix with aromatic vibrations and respond to ligand conformation and hydrogen bonding, their direction alone is not a decisive coordination criterion. Coordination of the imine nitrogens is established directly by diffraction.

Changes in the 1200–1300 cm^{-1} region are consistent with modification of the phenolic/phenoxide and aryl–oxygen environments. The ligand band near 1269 cm^{-1} is accompanied by features near 1275–1283 cm^{-1} in the complexes, while bands near 1220 and 1035 cm^{-1} remain prominent throughout the series. These regions include contributions from both the phenoxide framework and methoxy groups. The molecular formulas, donor connectivity and charge balance together support deprotonation of the two phenolic groups. Azide incorporation is readily recognized in **2** and **3**. Complex **2** has a characteristic high-intensity-region feature near 2098 cm^{-1}, whereas **3** has resolved bands near 2096 and 2058 cm^{-1} [22]. The additional feature in **3** is consistent with its greater variety of azide environments, including terminal and bridging coordination. Similarly, retention of acetate in **1** and **2** is structurally established. Its carboxylate vibrations overlap ligand bands in the 1400–1600 cm^{-1} region [23], preventing an unambiguous extraction of a single diagnostic separation between asymmetric and symmetric carboxylate stretches from these spectra. The dicyanamide compounds display closely corresponding multi-band patterns in the nitrile-containing region: 2326, 2262, 2210 and 2196 cm^{-1} for **4**, and 2325, 2262, 2212 and 2197 cm^{-1} for **5** [24]. These features distinguish the dicyanamide branch from the acetate and azide products.

Electronic absorption spectra

H_2L exhibits absorption maxima at 229, 257 and 345 nm, whereas the complexes have short-wavelength maxima near 225–226 and 246–247 nm and a longer-wavelength band near 377–380 nm (Figures S9-S14). The long-wavelength feature therefore shifts by approximately 32–35 nm after complex formation, while the intermediate ultraviolet band moves to shorter wavelength. These observations are compatible with substantial redistribution of the ligand electronic structure following phenolic deprotonation, metal coordination and conformational restriction.

Powder X-ray diffraction

The principal reflections of the experimental PXRD patterns are consistent with those simulated from the single crystal structures, supporting the correspondence between the bulk samples and the crystallographically characterized phases (Figures S15-S19).

Antibacterial activity

The antibacterial activities of H_2L and complexes 1–5 were evaluated against *Staphylococcus aureus*, *Bacillus subtilis*, *Pseudomonas aeruginosa* and *Escherichia coli* using the agar well diffusion method, with Gatifloxacin and Ciprofloxacin as reference antibiotics. The inhibition-

zone diameters are presented in Table **3** as mean ± standard error from three replicates. The mean zone diameters increased with increasing concentration wherever measurable inhibition was recorded. At 1.0 mg mL^{-1}, all five complexes produced larger mean inhibition zones than H_2L against each tested organism (Figure 6). The DMSO control showed no measurable inhibition.

Against the Gram-positive bacteria, the mean inhibition-zone diameters at 1.0 mg mL^{-1} followed the order **2** > **5** > **4** > **3** > **1**. Complex **2** produced the largest zones against *S. aureus* and *B. subtilis*, measuring 26 ± 4 and 28 ± 5 mm, respectively. The corresponding values were 24 ± 3 and 25 ± 5 mm for **5**, 23 ± 4 and 24 ± 6 mm for **4**, 20 ± 5 and 23 ± 5 mm for **3**, and 18 ± 5 and 20 ± 6 mm for **1**. H_2L gave smaller zones of 14 ± 3 and 15 ± 4 mm, respectively.

Against the Gram-negative bacteria, smaller mean inhibition zones were observed for each complex at 1.0 mg mL^{-1} than against the Gram-positive organisms. For *P. aeruginosa*, complexes **1**–**5** gave zone diameters of 18 ± 3, 20 ± 4, 17 ± 3, 17 ± 4 and 19 ± 3 mm, respectively, compared with 13 ± 3 mm for H_2L. For *E. coli*, complexes **2** and **5** shared the largest mean zone diameter among the complexes, with values of 18 ± 3 and 18 ± 4 mm, respectively. Complexes **1**, **3** and **4** produced zones of 15 ± 3, 14 ± 3 and 16 ± 3 mm, respectively, whereas H_2L gave 11 ± 3 mm.

The lowest tested concentrations producing measurable inhibition zones are summarized in Table 4. Complex **5** retained measurable inhibition against both Gram-positive organisms at 0.1 mg mL^{-1}, giving zones of 11 ± 3 mm against *S. aureus* and 12 ± 2 mm against *B. subtilis*. Complex **2** also inhibited *B. subtilis* at 0.1 mg mL^{-1}, with a zone diameter of 11 ± 2 mm, while its lowest tested concentration producing a measurable zone against *S. aureus* was 0.2 mg mL^{-1}. For complexes **3** and **4**, measurable inhibition against both Gram-positive organisms was recorded down to 0.2 mg mL^{-1}, compared with 0.4 mg mL^{-1} for **1**. Against *P. aeruginosa*, the lowest tested concentrations producing measurable zones were 0.4 mg mL^{-1} for **2**, **3** and **5**, and 0.6 mg mL^{-1} for **1** and **4**. Against *E. coli*, these concentrations were 0.4 mg mL^{-1} for **5**, 0.6 mg mL^{-1} for **2** and **4**, and 0.8 mg mL^{-1} for **1** and **3**. These values describe the observed concentration limits of the diffusion assay and should not be interpreted as MICs. All the five complexes have similar or better activities than the zinc complex with *N'*-(2-hydroxy-4-methoxybenzylidene)-3-methylbenzohydrazide as ligand [25].

At 1.0 mg mL^{-1}, complex **2** gave mean inhibition zones numerically close to those of the reference antibiotics against the Gram-positive organisms: Gatifloxacin produced zones of 26 ± 5 and 27 ± 6 mm, and ciprofloxacin produced zones of 24 ± 5 and 23 ± 3 mm against *S. aureus* and *B. subtilis*, respectively. Against the Gram-negative organisms, all five complexes gave smaller mean zones than either reference antibiotic. Both antibiotics produced measurable

inhibition against all four organisms at the lowest concentration reported for them, 0.2 mg mL^{-1}.

Conclusions

The H_2L/zinc acetate system accommodates a linear trinuclear acetate complex, two distinct tetranuclear azide assemblies and two dicyanamide-linked one-dimensional polymers. At fixed ligand:metal feed, increasing azide loading is associated with removal of acetate and a change from two five-coordinate zinc-site types to a five-/four-coordinate combination, while tetranuclearity is retained. In the dicyanamide branch, the same change in auxiliary-ligand loading is associated with replacement of a bent trinuclear chain unit by a dinuclear unit, while one-dimensional propagation is retained. These outcomes demonstrate that stoichiometry-dependent structural selection involves donor allocation and auxiliary-ligand retention as well as nuclearity. Antibacterial diffusion screening identifies **2** as the strongest Gram-positive candidate by mean zone diameter at 1.0 mg mL^{-1}, with **5** also showing low-dose responses. Although the complexes were introduced as DMSO solutions in the agar-diffusion assay, their speciation and stability under the assay conditions were not determined. The antibacterial results are therefore treated as preliminary screening data; no assignment of the active solution species or structure–activity relationship is made. Solution-state characterization remains an important subject for future study.

Declaration of competing interest

The authors declare that they have no known competing financial interests or personal relationships that could have appeared to influence the work reported in this paper.

Appendix A. Supplementary data

CCDC 2595924–2595928 contain the supplementary crystallographic data for the complexes. These data can be obtained free of charge *via* http://www.ccdc.cam.ac.uk/conts/retrieving.html, or from the Cambridge Crystallographic Data Centre, 12 Union Road, Cambridge CB2 1EZ, UK; fax: (+44) 1223-336-033; or e-mail: deposit@ccdc.cam.ac.uk.

Funding Declaration

There is no funding for this work.

References

[1] Malav R, Ray S (2025) RSC Adv 15:22889

[2] Mohan RD, Sarukrishna S, Babu AS, Santhosh D, Fathima SA, Parvathy B (2026) Inorg

Chim Acta 590:122980
[3] Takhar P, Chhapoliya M, Janmeda P, Singh D (2026) Coord Chem Rev 564:218001
[4] Fallah-Mehrjardi M, Kargar H, Munawar KS, Ashfaq M (2025) J Mol Struct 1342:142760
[5] Rana MS, Rayhan NMA, Emad A, Hossain MI, Shah MM, Kudrat-E-Zahan M, Hossen MF, Asraf MA (2025) J Coord Chem 78:937
[6] Sindhu S, Singh F, Kumar RS, Arockiasamy S (2025) Inorg Chim Acta 577:122502
[7] Liang XX, Zhao XY, Guo A, Wang XW, Rong M, Chang L, Sun ZQ, Jin XD (2023) J Coord Chem 76:307
[8] Middya P, Frontera A, Chattopadhyay S (2024) RSC Adv 14:13905
[9] You ZL, Hou P, Ni LL, Chen S (2009) Inorg Chem Commun 12:444
[10] Karmakar M, Frontera A, Chattopadhyay S (2020) CrystEngComm 22:6876
[11] Zhang L, Gu YQ, Feng XH, Yang T, Li XY, Wang J, You ZL (2022) Acta Chim Slov 69:674
[12] Tabrizi L, Chiniforoshan H, Mcardle P (2015) J Coord Chem 68:1936
[13] Kumar R, Singh AA, Kumar U, Jain P, Sharma AK, Kant C, Faizi CMSH (2023) J Mol Struct 1294:136346
[14] Kaczmarek MT, Zabiszak M, Nowak M, Jastrzab R (2018) Coord Chem Rev 370:42
[15] Su YX, Huang J, Yang K, Zhang Y, Wei KJ, Liu GH (2026) J Mol Struct 1367 :146168
[16] Wang CC, Wang JH, Wang G, Li CW, Wang LL, Ong SK (2026) J Mol Struct 1350:144059
[17] Slassi S, El-Ghayoury A, Aarjane M, Yamni K, Amine A (2020) Appl Organomet Chem 34:e5503
[18] Sheldrick GM (2015) Acta Crystallogr A71:3
[19] Sheldrick GM (2015) Acta Crystallogr C71:3
[20] Ghosh M, Fleck M, Mahanti B, Ghosh A, Pilet G, Bandyopadhyay D (2012) J Coord Chem 65:3884
[21] Addison AW, Rao TN, Reedijk J, van Rijn J, Verschoor GC (1984) J Chem Soc Dalton Trans 7:1349
[22] Basak S, Sen S, Banerjee S, Mitra S, Rosair G, Rodriguez MTG (2007) Polyhedron 26:5104
[23] Bhardwaj VK, Hundal MS, Corbella M, Gómez V, Hundal G (2012) Polyhedron 38:224
[24] Talukder P, Shit S, Sasmal A, Batten SR, Moubaraki B, Murray KS, Mitra S (2011) Polyhedron 30:1767
[25] Mao FL (2026) Inorg Chim Acta 594:123094.

Table 1. Crystal data and refinement parameters for complexes **1**–**5**.

Parameter	**1**	**2**	**3**	**4**	**5**
Chemical formula	$C_{48}H_{54}N_4O_{12}Zn_3$	$C_{48}H_{54}N_{10}O_{12}Zn_4$	$C_{44}H_{48}N_{16}O_8Zn_4$	$C_{48}H_{48}N_{10}O_8Zn_3$	$C_{26}H_{24}N_8O_4Zn_2$
Formula weight	1075.06	1224.49	1190.46	1089.07	643.27
Crystal dimensions (mm)	0.26 × 0.23 × 0.22	0.26 × 0.25 × 0.25	0.18 × 0.18 × 0.16	0.25 × 0.23 × 0.20	0.22 × 0.20 × 0.19
Crystal system	Monoclinic	Triclinic	Triclinic	Monoclinic	Triclinic
Space group	$P2_1/c$	$P\bar{1}$	$P\bar{1}$	$P2/c$	$P\bar{1}$
a (Å)	9.5894(7)	11.142(1)	9.672(1)	12.440(1)	10.627(2)
b (Å)	11.5582(8)	11.816(1)	10.804(1)	11.728(1)	11.281(2)
c (Å)	21.363(1)	11.992(1)	13.281(1)	17.049(2)	14.624(2)
α (°)	90	61.766(1)	110.823(1)	90	73.934(2)
β (°)	100.181(1)	76.586(1)	101.854(2)	98.162(2)	85.827(2)
γ (°)	90	72.185(1)	101.866(1)	90	62.898(2)
Volume (Å^3)	2330.5(3)	1317.1(2)	1209.2(2)	2462.1(4)	1496.7(3)
Z	2	1	1	2	2
Calculated density (g cm^{-3})	1.532	1.544	1.635	1.469	1.427
μ (mm^{-1})	1.599	1.869	2.030	1.512	1.646
F(000)	1112	628	608	1120	656
Data collection temperature (K)	298(2)	298(2)	298(2)	298(2)	298(2)
θ_{max} (°)	25.50	25.50	25.50	25.50	25.50
Measured reflections	12220	7162	6546	12717	8099
Independent reflections	4335	4849	4445	4582	5492
Observed reflections [$I > 2\sigma(I)$]	3288	3827	3251	2158	3460
Completeness to θ_{full} (%)	99.9	98.9	99.0	99.8	98.9
Parameters	362	448	327	367	363
Restraints	244	406	0	96	0
Goodness of fit on F^2	1.021	1.091	1.056	1.003	1.042
R_1, wR_2 [$I > 2\sigma(I)$][a]	0.0338,	0.0398,	0.0430,	0.0545,	0.0730,

Parameter	**1**	**2**	**3**	**4**	**5**
R_1, wR_2 (all data)[a]	0.0798 0.0530, 0.0891	0.1080 0.0547, 0.1169	0.1034 0.0658, 0.1166	0.1347 0.1389, 0.1766	0.2167 0.1141, 0.2537

[a] $R_1 = \Sigma||F_o| - |F_c||/\Sigma|F_o|$; wR_2 and goodness of fit are based on F^2.

Table 2. Selected bond lengths (Å), bond angles (°) for complexes **1**–**5**.

Parameter	**1**	**2**	**3**	**4**	**5**
Zn1–O (ligand)	O1 2.0254(19); O2 2.002(2)	O1 2.023(3); O2 2.024(3)	O1 2.023(3); O2 2.007(3)	O1 1.996(5); O2 1.990(4)	O1 2.000(5); O2 1.997(5)
Zn1–N (imine)	N1 2.035(2); N2 2.055(2)	N1 2.038(3); N2 2.024(3)	N1 2.052(3); N2 2.038(3)	N1 2.049(5); N2 2.051(6)	N1 2.044(6); N2 2.083(6)
Zn1–X (auxiliary donor)	O5 1.977(2) (OAc)	O5 1.995(3) (OAc)	N3 2.040(4) (azide)	N3 1.990(6) (dca)	N3 1.986(7) (dca)
Zn2–O (ligand)	O1 2.1380(19); O2 2.1207(17)	O1 2.101(2); O2 2.001(3)	O1 1.956(3); O2 1.982(3)	O1 2.134(4); O2 2.151(5)	O1 2.044(5); O2 2.020(5)
Zn2–X (auxiliary donor)[a]	O6 2.071(2) (OAc)	O6 2.009(3) (OAc); N3 2.050(3), 2.109(3) (azide)	N6 1.966(5); N3 1.981(3) (azide)	N5 2.077(6) (dca)	N5 1.996(7); N6 2.043(8); N8 2.105(8) (dca)
C=N	N1–C7 1.266(4); N2–C14 1.270(4)	N1–C7 1.272(5); N2–C14 1.278(6)	N1–C7 1.282(5); N2–C14 1.274(5)	N1–C7 1.253(8); N2–C14 1.270(8)	N1–C7 1.274(10); N2–C14 1.279(9)

Parameter	**1**	**2**	**3**	**4**	**5**
Zn1···Zn2 (Å)	2.9806(3)	2.9148(6)	3.0806(7)	3.1480(9)	3.1276(13)
Zn1–O–Zn2 (°)	91.39(8), 92.57(8)	89.92(10), 92.81(11)	101.46(12), 101.10(12)	99.3(2), 98.9(2)	101.3(2), 102.3(2)
Zn1–Zn2–Zn1 (°)	180	–	–	109.05(4)	–
Zn–N–Zn azide bridge (°)	–	102.57(15) (Zn2–N3–Zn2)	124.35(17) (Zn2–N3–Zn1)	–	–

[a] X denotes the auxiliary acetate, azide or dicyanamide donor.

Table 3. Antibacterial activity of the tested materials (IZD (mean ± standard error) (mm))[a].

Dose (mg mL^{-1})	*Staphylococcus aureus*	*Bacillus subtilis*	*Pseudomonas aeruginosa*	*Escherichia coli*
H_2L				
1.0	14±3	15±4	13±3	11±3
0.8	13±3	12±3	11±3	–
0.6	11±2	–	–	–
1				
1.0	18±5	20±6	18±3	15±3
0.8	15±3	16±3	15±3	11±2
0.6	13±3	13±4	12±3	–
0.4	10±3	11±3	–	–
2				
1.0	26±4	28±5	20±4	18±3
0.8	22±4	25±4	18±3	13±2
0.6	19±3	21±4	14±4	11±3
0.4	16±3	18±3	10±3	–
0.2	12±3	14±3	–	–
0.1	–	11±2	–	–
3				
1.0	20±5	23±5	17±3	14±3
0.8	18±5	19±4	16±3	10±3
0.6	14±4	16±4	12±2	–

0.4	12±4	13±4	10±3	–
0.2	11±3	10±3	–	–
4				
1.0	23±4	24±6	17±4	16±3
0.8	21±5	20±5	14±4	14±3
0.6	18±3	19±4	10±3	11±3
0.4	15±3	15±4	–	–
0.2	12±3	13±3	–	–
5				
1.0	24±3	25±5	19±3	18±4
0.8	22±4	23±5	15±3	16±4
0.6	19±4	20±3	12±3	13±3
0.4	15±3	17±3	10±3	11±3
0.2	13±3	14±3	–	–
0.1	11±3	12±2	–	–
Gatifloxacin				
1.0	26±5	27±6	25±4	26±4
0.8	23±4	23±4	22±3	24±5
0.6	20±5	19±5	18±4	21±3
0.4	18±6	15±3	15±4	16±3
0.2	16±4	14±4	12±3	13±4
Ciprofloxacin				
1.0	24±5	23±3	21±3	25±3
0.8	21±5	22±3	20±3	24±5
0.6	18±6	18±4	17±4	19±6
0.4	15±4	15±5	14±3	14±4
0.2	11±3	12±3	11±3	10±3
DMSO				
1.0	–	–	–	–

[a] Values in mm, mean ± SD, n = 3. A dash denotes no reported measurable zone.

Table 4. Lowest tested concentrations (mg mL^{-1}) producing measurable inhibition zones in the agar well diffusion assay[a].

	Staphylococcus aureus	*Bacillus subtilis*	*Pseudomonas aeruginosa*	*Escherichia coli*
H_2L	0.6	0.8	0.8	1.0
1	0.4	0.4	0.6	0.8
2	0.2	0.1	0.4	0.6
3	0.2	0.2	0.4	0.8
4	0.2	0.2	0.6	0.6
5	0.1	0.1	0.4	0.4
Gatifloxacin	0.2	0.2	0.2	0.2
Ciprofloxacin	0.2	0.2	0.2	0.2

[a] These values represent the lowest concentrations with measurable inhibition zones among those reported in Table 3 and should not be interpreted as MICs.

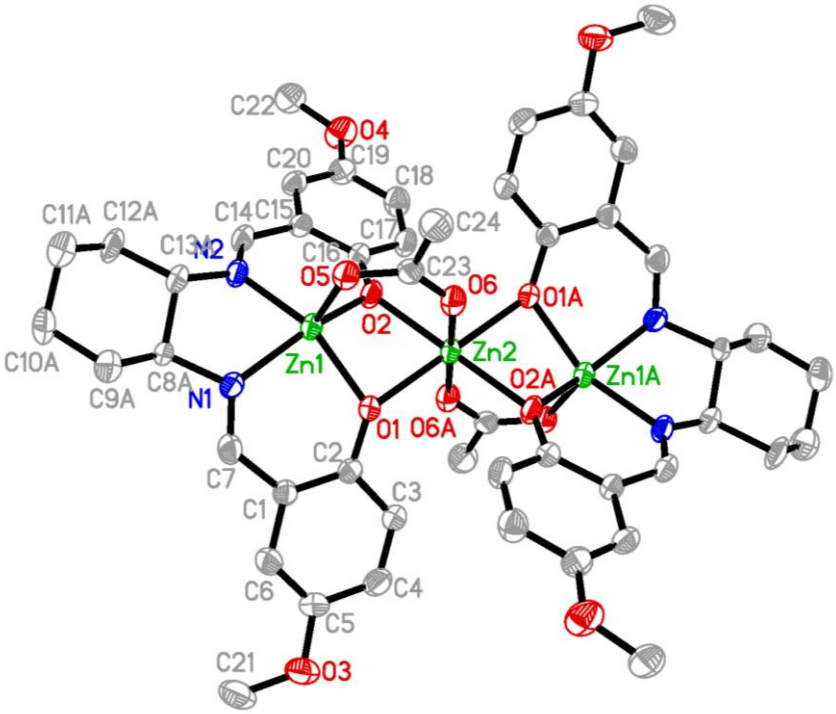


Figure 1. Molecular structure of **1** with 30% probability thermal ellipsoids. Hydrogen atoms are omitted for clarity. Symmetry operation for A: $1 - x$, $1 - y$, $1 - z$.

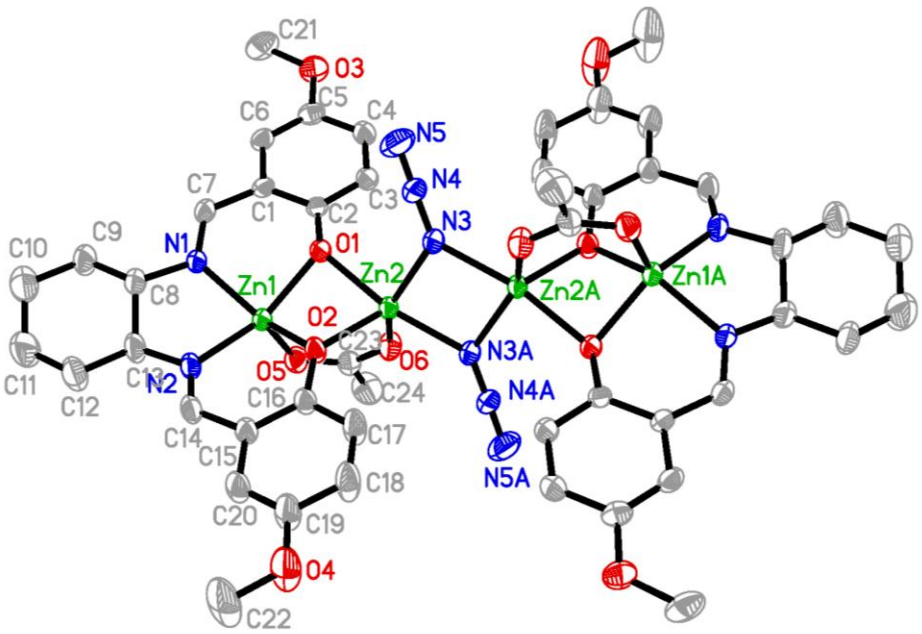


Figure 2. Molecular structure of **2** with 30% probability thermal ellipsoids. Hydrogen atoms are omitted for clarity. Symmetry operation for A: $1 - x$, $2 - y$, $1 - z$.

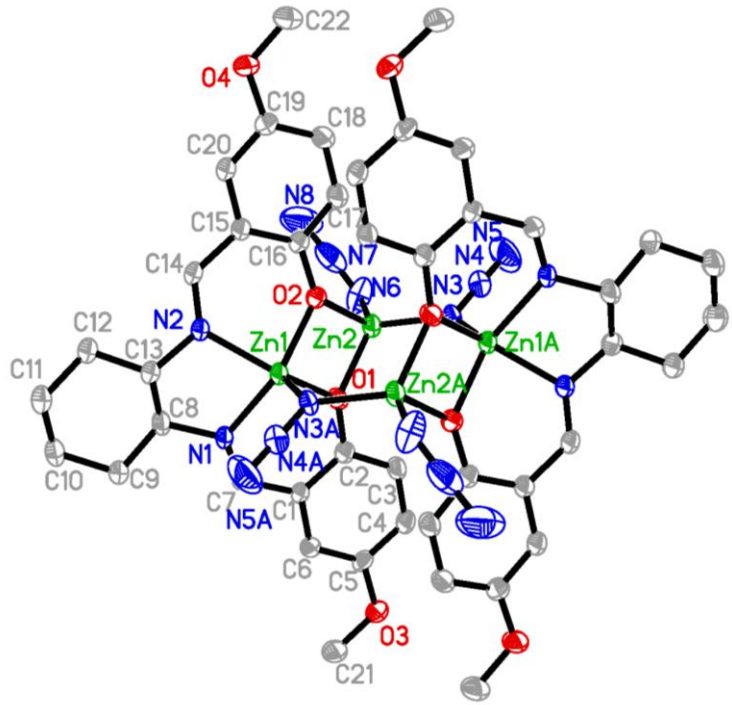


Figure 3. Molecular structure of **3** with 30% probability thermal ellipsoids. Hydrogen atoms are omitted for clarity. Symmetry operation for A: $1 - x$, $1 - y$, $1 - z$.

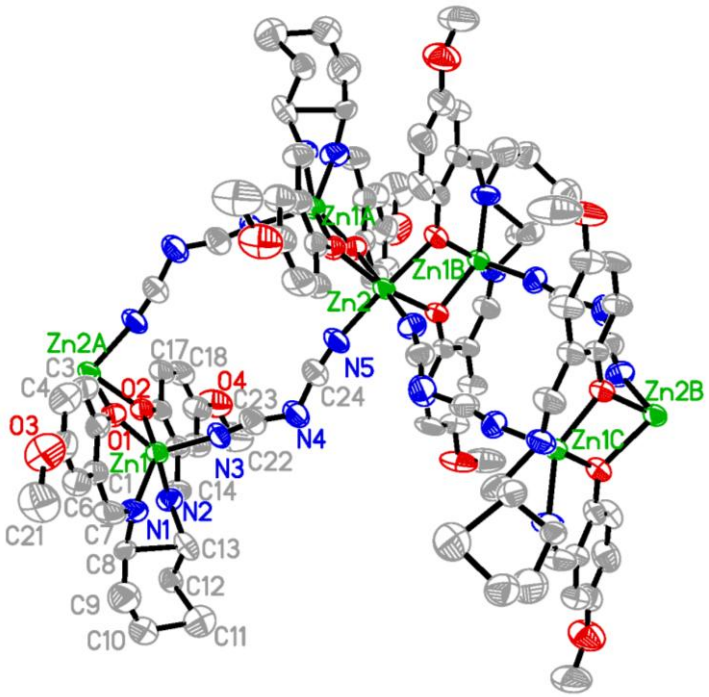


Figure 4. Molecular structure of **4** with 30% probability thermal ellipsoids. Hydrogen atoms are omitted for clarity. Symmetry operation for A: $1 - x$, $2 - y$, $1 - z$; B: x, $2 - y$, $1/2 + z$.

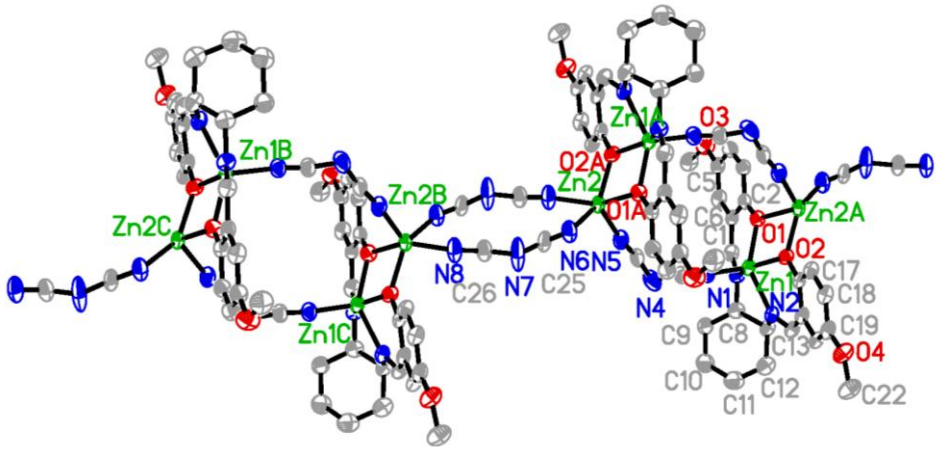


Figure 5. Molecular structure of **5** with 30% probability thermal ellipsoids. Hydrogen atoms are omitted for clarity. Symmetry operations for A and B: $1 - x$, $1 - y$, $1 - z$; $1 - x$, $2 - y$, $- z$.

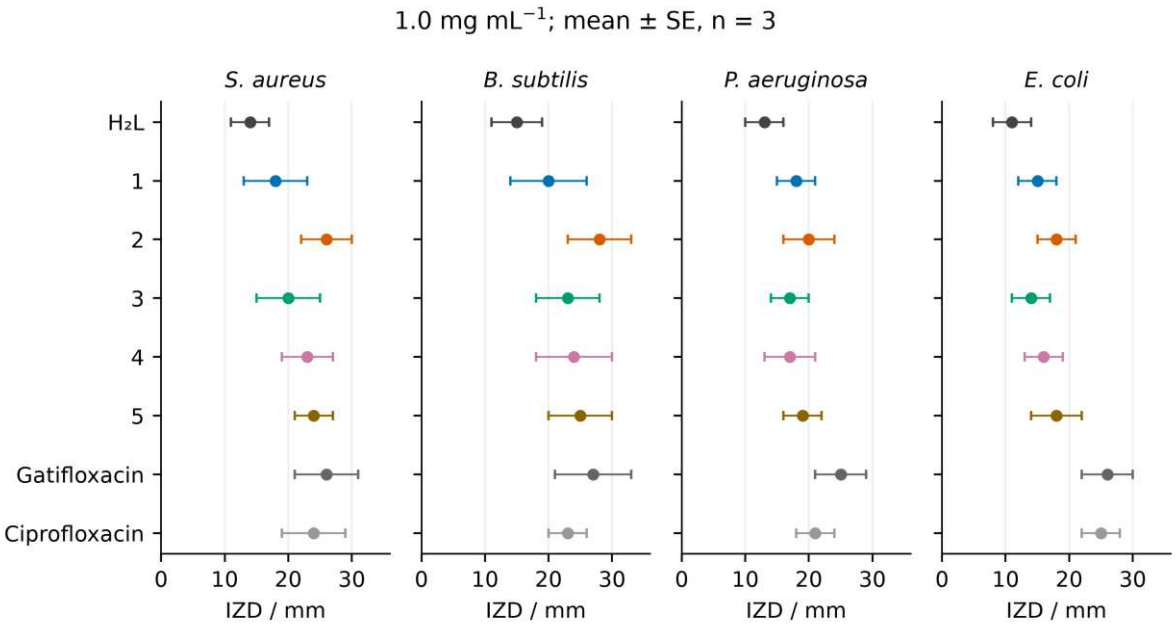


Figure 6. Inhibition-zone diameters at 1.0 mg mL^{-1} against the four test organisms. Points and bars show the reported mean ± standard error for three replicates.

Supplementary Files

This is a list of supplementary files associated with this preprint. Click to download.

- SupplementaryInformation.docx